OQAM/IOTA Downlink Air Interface for 3G/4G

Peter Jung
Fraunhofer German-Sino Lab for Mobile Communications (MCI)
and the Heinrich-Hertz Institute
jung@hhi.fraunhofer.de

1 Introduction

In order to provide higher data rates in the UMTS (3G) downlink, the High Speed Downlink Packet Access (HSDPA), was standardized in UMTS Release 5. However, to support high data rates in the WCDMA system smaller spreading factors are used to handle the shared access. Using higher modulation constellations data rates beyond 10Mbps are then achievable. On the other hand, by decreasing the spreading factor more intersymbol interference caused by the time-dispersive channel is introduced which can only be managed by advanced WCDMA receivers. This increase in complexity has initiated a reinspection of the physical layer. In particular it is known that Orthogonal Frequency Division Multiplexing (OFDM) has the capability to resolve the inherent structure of time-invariant (or slowly fading) channels, i.e. converts the frequency-selective channel into flat fading channels on the corresponding subcarriers. From mathematical point of view the joint transmitter and receiver signaling (that includes a appropriate cyclic prefix) diagonalizes a complete class of linear time-invariant channels on a very low complexity level. Moreover with frequency-selective channel information available at the transmitter it is expected that OFDM with time-frequency scheduling is superior to WCDMA employing time scheduling only. It was already observed that twice the averaged throughput is achievable using multidimensional scheduling [1]. Therefore OFDM was proposed in the 3G Partnership Project (3GPP) as an alternative air interface [2]. The conventional OFDM scheme can be extended in several ways to match the requirements for more mobility and increased bandwidth efficiency. In particular an approach based on Offset QAM in conjunction with Gaussian-like pulse shapes (OQAM/IOTA) [3], also incorporated in the 3GPP OFDM study item, reflects a promising new direction. Due to the enhancement of the physical layer an improvement of the overall system performance is expected while the air interface is still very similar to OFDM. Hence, strategies on adaptive modulation, coding and time-frequency scheduling developed for OFDM can be applied without major modifications. The purpose of this paper is

to compare the physical layer capabilities of both system designs in 3GPP propagation scenarios and demonstrate the potentials of OQAM/IOTA.

The paper is organized as follows. In the first part both multicarrier schemes are reviewed showing the connection to Gabor's time-frequency signaling. Then the principles of WSSUS pulse adaption are presented. Finally several performance evaluations are shown and discussed in the 3GPP context.

2 System Model

Conventional OFDM and pulse shaped OQAM can be jointly formulated using the concept of generalized multicarrier schemes. In this framework the baseband transmit signal is

$$s(t) = \sum_{(mn)\in\mathcal{I}} e^{i2\pi mFt}\gamma(t-nT) = \sum_{(mn)\in\mathcal{I}} \gamma_{mn}(t) \tag{1}$$

where i is the imaginary unit and $\gamma_{mn} := \boldsymbol{S}_{(nT,mF)}\gamma$ is a time-frequency shifted version of the transmit pulse γ, i.e. shifted according to the lattice $T\mathbb{Z} \times F\mathbb{Z}$. Due to this rectangular lattice in the time-frequency plane, this setup is sometimes called Gabor signaling. The sampling density is related to the bandwidth efficiency (in symbols) of the signaling, i.e. $\epsilon := (TF)^{-1}$.

The coefficients x_{mn} are the complex data symbols at time instant n and subcarrier index m with the property $\mathbf{E}\{\boldsymbol{x}\boldsymbol{x}^*\} = \mathbb{I}$ ($\cdot^*$ means conjugate transpose). The indices (mn) range over the doubly-countable index set $\mathcal{I}$, referring to the data burst to be transmitted. We will denote the linear time-variant channel by $\boldsymbol{\mathcal{H}}$ and the additive white Gaussian noise process (AWGN) by $n(t)$. The received signal is then

$$r(t) = (\boldsymbol{\mathcal{H}}s)(t) + n(t) = \int (\boldsymbol{\Sigma}_{(\tau,\nu)}\boldsymbol{S}_{(\tau,\nu)}s)(t)d\tau d\nu + n(t) \tag{2}$$

with $\boldsymbol{\Sigma}_{(\tau,\nu)}$ being a realization of the (causal) channels spreading function of finite support $[0,\tau_d] \times [-B_D, B_D]$. We used here the notion of the WSSUS channel and its decomposition into time-frequency shifts. In the WSSUS assumption the channel is characterized by the second order statistics of $\boldsymbol{\Sigma}_{(\tau,\nu)}$, i.e. the scattering function $\boldsymbol{C}_{(\tau,\nu)}$

$$\mathbf{E}\{\boldsymbol{\Sigma}_{(\tau,\nu)}\boldsymbol{\Sigma}^*_{(\tau',\nu')}\} = \boldsymbol{C}_{(\tau,\nu)}\delta(\tau-\tau')\delta(\nu-\nu') \tag{3}$$

Moreover we assume $\mathbf{E}\{\boldsymbol{\Sigma}_{(\tau,\nu)}\} = 0$. To obtain the data symbol $\tilde{x}_{kl}$ the receiver does the projection on $g_{kl} := \boldsymbol{S}_{(lT,kF)}g$, i.e.

$$\tilde{x}_{kl} = \langle g_{kl}, r\rangle = \int e^{-i2\pi kFt}\overline{g}(t-lT)r(t)dt \tag{4}$$

By introducing the elements $H_{kl,mn} := \langle g_{kl}, \boldsymbol{\mathcal{H}}\gamma_{mn}\rangle$ of the channel matrix $H \in C^{\mathcal{I}\times\mathcal{I}}$, the multicarrier transmission can be formulated as the linear equation $\tilde{\boldsymbol{x}} = H\boldsymbol{x} + \boldsymbol{n}$, where $\boldsymbol{n}$ is the vector of the projected noise having power of σ^2 per component. If we assume that the receiver has perfect channel knowledge (given by $\boldsymbol{\Sigma}_{(\tau,\nu)}$ a full single carrier based zero forcing equalization would be of the form $\tilde{x}_{kl}^{\text{eq}} = H_{kl,kl}^{-1}\tilde{x}_{kl}$ (or alternatively MMSE equalization if the noise variance is known). Using the commutation relations

$$\boldsymbol{S}_{(\tau,\nu)}\boldsymbol{S}_{(lT,kF)} = e^{-i2\pi(\tau kF-\nu lT)}\boldsymbol{S}_{(lT,kF)}\boldsymbol{S}_{(\tau,\nu)} \tag{5}$$

one easily arrives at

$$\begin{aligned} H_{kl,kl} = \langle g_{kl}, \boldsymbol{\mathcal{H}}\gamma_{kl}\rangle &= \int \boldsymbol{\Sigma}_{(\tau,\nu)}\rangle g_{kl}, \boldsymbol{S}_{(\tau,\nu)}\gamma_{kl}\rangle d\tau d\nu \\ &=: \int \boldsymbol{\Sigma}_{(\tau,\nu)} e^{-i2\pi(\tau kF-\nu lT)}\mathbf{A}_{g\gamma}(\tau,\nu)d\tau d\nu \end{aligned} \tag{6}$$

where $\mathbf{A}_{g\gamma}(\tau,\nu) :=\rangle g, \boldsymbol{S}_{\tau,\nu}\gamma >$ is the cross ambiguity function of the pulse pair $\{g,\gamma\}$. (non-diagonal elements of H are given similar). Thus, the complex channel coefficient $H_{kl,kl}$ is given by the (symplectic) 2D Fourier transform of the channels spreading function weighted by the cross ambiguity function of $\{g,\gamma\}$.

2.1 The cp-OFDM Approach

The classical OFDM system exploiting a cyclic prefix (cp-OFDM) is obtained by setting γ to the rectangular pulse:

$$\gamma(t) = \frac{1}{\sqrt{T_u + T_{cp}}}\chi_{[-T_{cp},T_u]}(t). \tag{7}$$

The function $\chi_{[-T_{cp},T_u]}$ is the characteristic function of the interval $[-T_{cp}, T_u]$, where T_u denotes the length of the useful part of the signal and T_{cp} the length of the cyclic prefix, hence the OFDM overall symbol period is $T := T_u + T_{cp}$. The OFDM subcarrier spacing is $F = 1/T_u$. At the OFDM receiver the rectangular pulse $g(t) = \frac{1}{\sqrt{T_u}}\chi_{[0,T_u]}(t)$ is used which removes the cyclic prefix. The time-frequency density of this signaling is given by the spectral efficiency $\varepsilon = (TF)^{-1} = T_u/(T_u + T_{cp}) < 1$. It can be easily verified that $\mathbf{A}_{g\gamma}(\tau + nT, mF) = \sqrt{\epsilon}\delta_{n0}\delta_{m0}$ if $0 \leqslant \tau \leqslant T_{cp}$. i.e. it represents the orthogonality relation $\langle g_{kl}, \gamma_{mn}\rangle = \delta_{km}\delta_{ln}$. Moreover this implies, that the orthogonality holds for all channel realization as long as the scattering function fulfills $B_D = 0$ and $\tau_d \leqslant T_{cp}$, i.e.

$$H_{kl,mn} = \langle g_{kl}, \mathbf{H}\gamma_{mn}\rangle = \sqrt{\epsilon}\delta_{km}\delta_{ln}\hat{h}(kF) \tag{8}$$

where $\hat{h}(f)$ is the Fourier transform of the impulse response $h(\tau) = \boldsymbol{\Sigma}_{(\tau,0)}$ that corresponds to the time-invariant channel. Therefore cp-OFDM is a

powerful signaling, which diagonalizes time-invariant channels, but at the cost of signal power and bandwidth efficiency. This does not hold anymore if the channels are doubly-dispersive, as for example modeled by the WSSUS assumptions. Hence in high mobility scenarios intercarrier interference (ICI) limits the performance. Normally ICI can be reduced by the use of smoother pulses and enough decay in the frequency domain. But one of the deeper results in Gabor theory, namely the Balian-Low Theorem (see for example [4]), states that orthogonal (or biorthogonal) pulses at $TF \approx 1$ must have bad time-frequency localization properties (at $TF = 1$ either diverging temporal or spectral localization). Indeed, in discrete implementation the localization of orthogonalized Gaussians for $\epsilon \leqslant 1$ and "tighten" Gaussians for $\varepsilon \geqslant 1$ peaks at the critical density $(TF)^{-1} = 1$ and drops down, so that pulse shaping is hand-able only for $TF \leqslant 1/2$ or $TF \geqslant 2$. Therefore pulse shaping is mainly prohibited for efficient cp-OFDM-like transmission if still (bi-)orthogonality is desired.

2.2 The Pulse Shaped OQAM/OFDM Approach

The first idea of OQAM based modulation for OFDM (also known as OFDM/OQAM) was proposed by Chang [5] and design aspects where later presented by Saltzberg [6]. The historical motivation of this scheme was the proposal of an efficient multicarrier signaling that includes (spectral) overlapping pulses. This modulation is obtained in (1) and (4), if the time-frequency density is given as $TF = 1/2$ and the mappings $x_{mn} = i^{m+n} x^R_{mn}$ before modulation and $\tilde{x}^R_{mn} = \Re\{-i^{m+n}\, \tilde{x}_{mn}\}$ after demodulation are performed, where $x^R_{mn} \in R$ is the real-valued information to transmit. Note that there is no such relation for OQAM based multicarrier transmission equivalent to (8) for cp-OFDM. Hence also in time-invariant channels there will be ICI. But in the absence of a channel biorthogonality of the form $\Re\{< g_{mn}, \gamma_{kl} >\} = \delta_{mk}\delta_{nl}$ can be achieved. Furthermore it is known that the design of orthogonal OQAM based multicarrier transmission (OQAM/OFDM) is equivalent to the design of orthogonal Wilson bases. Because the system operates at $TF = 1/2$ with transmission of real information for complex information the effective efficiency is 1 but pulse shaping is possible.

3 Pulse Adaption

3.1 WSSUS Pulse Shaping Principles

Normally in multicarrier transmission only single carrier equalization is considered, hence it is naturally to require $a := |H_{kl,kl}|^2$ (the channel gain) to be maximal and the interference power $b := \sum (kl) \neq (mn)|^2$ to be minimal as possible. This addresses the concept of *pulse shaping*, hence to find good pulses $\{g, \gamma\}$ such that its cross ambiguity yields maximum channel

gain and minimum interference power. However it is much more realistic to adapt the pulses only to the second order statistics, given by $\boldsymbol{C}_{(\tau,\nu)}$ and **not** to a particular channel realization $\boldsymbol{\Sigma}_{(\tau,\nu)}$. The full maximization of the

$$\text{SINR} = \frac{\mathbf{E}_{\boldsymbol{\mathcal{H}}}\{a\}}{\sigma^2 + \mathbf{E}_{\boldsymbol{\mathcal{H}}}\{b\}} \tag{9}$$

is rather complex to solve. However iterative methods are given in [7]. Moreover in [7] the connection to the simplified pulse design criterion [8]

$$\{\gamma^{(\text{opt})}, g^{(\text{opt})}\} = \arg\max_{(\gamma,g)} \int \boldsymbol{C}_{(\tau,\nu)} |\mathbf{A}_{g\gamma}(\tau,\nu)|^2 d\tau d\nu = \mathbf{E}_{\boldsymbol{\mathcal{H}}}\{a\} \tag{10}$$

for $g = \gamma = 1$, is shown.

3.2 Pulse Scaling

The latter optimization problem is still difficult to solve analytical, but the following second order approximation yields a simpler pulse design criterion. If we assume $g(t)$ and $\gamma(t)$ to be even and real, the squared cross ambiguity can be approximated for small τ and ν as follows

$$|\mathbf{A}_{g\gamma}(\tau,\nu)|^2 \approx \langle g,\gamma\rangle^2 \cdot (1 - 2\pi^2\nu^2\sigma_t^2 - 2\pi^2\tau^2\sigma_f^2) \tag{11}$$

with $\sigma_t^2 = \langle t^2 g,\gamma\rangle / \langle g,\gamma\rangle$ and $\sigma_f^2 = \langle f^2\hat{g},\hat{\gamma}\rangle / \langle g,\gamma\rangle$. The latter is a small extension of the often used approximation for the auto-ambiguity function ($g = \gamma$), which gives ellipses as contour lines of (11) in the (τ,ν)-plane. In [9] it was shown that using (11) in (10), $g = \gamma$ and assume flat rectangular or elliptic shape of $\boldsymbol{C}_{(\tau,\nu)}$ the extremal value is attained at

$$\sigma_t/\sigma_f = \tau_d/(2B_D) \tag{12}$$

Further for arbitrary scattering profiles exhibiting elliptical symmetry it was shown, that Hermite functions are local optima. Motivated by the last arguments we would use Gaussian (first Hermite function) properly scaled to channel statistics. Unfortunately this does not guarantee maximum SINR, i.e. only maximizes a lower bound to SINR (see [7] for more details). Only if $\{\gamma_{mn}\}$ is a tight frame, equality is given. Hence, the idea is to use indeed scaled Gaussian $d(t) \sim e^{-\pi\frac{2B_D}{\tau_d}t^2}$ which already fulfills (12) and to further minimize the interference by creating the tight pulse $\gamma(t)$ from $d(t)$, i.e. the pulse that creates a tight Gabor frame at $TF = 1/2$, which also will fulfill (12). Moreover this is needed to construct an orthogonal Wilson basis [10], i.e. orthogonal pulses for OQAM/OFDM.

3.3 Grid Scaling and Orthogonalization

Before creating a tight Gabor frame the time-frequency lattice has to be fixed now. The joint scaling rule is then.

$$\sigma_t/\sigma_f = T/F = \tau_d/(2B_D) \tag{13}$$

With the definition of the operator S_d

$$(S_d f)(t) := \sum_{(mn)\in\mathbb{Z}^2} \langle d_{mn}, f\rangle d_{mn}(t) \tag{14}$$

where $d_{mn} := \boldsymbol{S}_{(nT,mF)}d$, the tight pulse is given as $\gamma := S_d^{-1/2}d$ [4]. If $\{d_{mn}\}$ constitute a frame S_d is called frame operator. In particular for Gaussians the method proposed in [11] can also be used, which yields a tight frame too. But note that the latter does not hold anymore in the general case [12]. In the context of full complex pulseshaped multicarrier systems (no OQAM) this orthogonalization procedure was established also for more efficient lattice structures (see LOFDM, [13]) Furthermore because of the integer oversampling (of two) the calculation of $S_d^{-1/2}$ simplifies much in the Zak-domain and can be done using efficient FFT-based methods [14]. For the resulting tight pulse $\gamma(t)$ we will use the 3GPP common name *IOTA pulse* (IOTA= Isotropic Orthogonal Transform Algorithm), hence the system is called OQAM/IOTA. Finally the result of the orthogonalization of gaussian is shown in Fig.1.

3.4 With Bandwidth Constraint

Under a fixed bandwidth constraints W and fixed bandwidth efficiency ε (in complex symbols) the scaling rule (12) can be easily transformed into an optimal number of subcarriers as follows. Starting from the conditions $TF = \varepsilon$ for a given ε, $T/F = \tau_d/(2B_D)$ for a given channel statistics and $F = W/N$ for a fixed bandwidth, where N is the number of subcarriers, one gets

$$N = W\sqrt{\frac{\tau_d}{2\varepsilon \cdot B_D}} = \sqrt{\frac{\tau_d c}{2\varepsilon \cdot v f_c}} \tag{15}$$

where v is the speed between transmitter and receiver, c the speed of light and f_c the carrier frequency. In practical implementation via FFT and polyphase filtering N has be a power of 2,

For application of OQAM/IOTA in the context of UMTS HSDPA, hence using $\varepsilon = (TF)^{-1} = 2$, $f_c = 2$GHz, $W = 7.68$MHz, it turns out via (2) that $N = (256,)512, 1025, 2048(, 4096)$ are feasible (see Fig.2). The rule (2) represents nothing more than the tradeoff between time and frequency division multiplexing in time-variant channels.

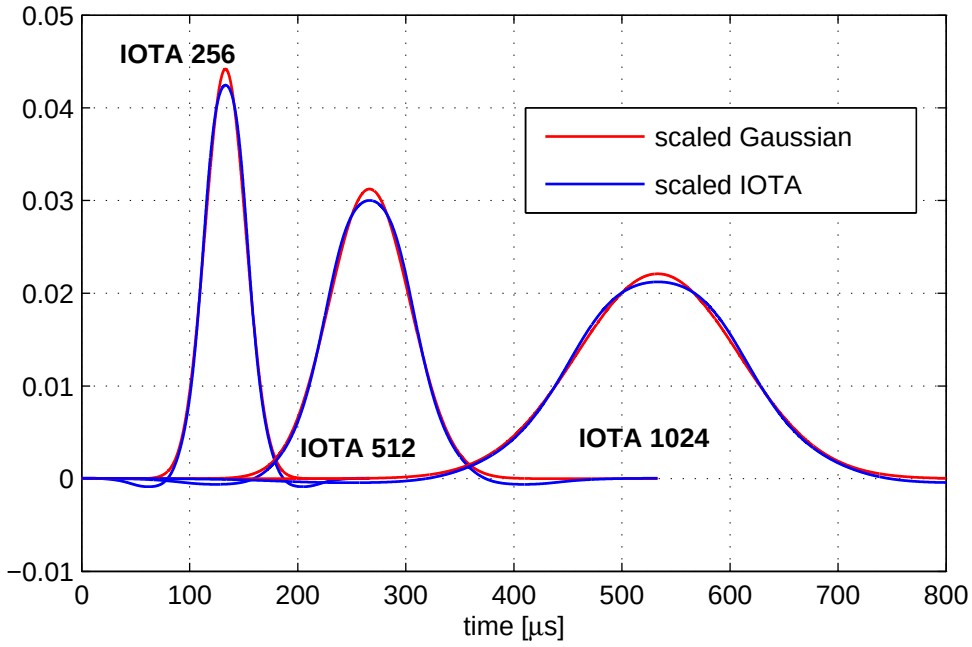

Figure 1: Creating tight frames from gaussians

4 Implementation Aspects

Before we start with performance discussion, we will make some notes on the practical problem of ideal channel estimation and quantify the complexity increase of OQAM/IOTA.

4.1 Ideal Channel Estimation

Cyclic prefix cp-OFDM provides a simple relation of the channel coefficient $H_{kl,kl}$ to the transfer function of channel given by (8). For pulse shaped OQAM this does hold only in an approximate sense. In this performance comparison the two multicarrier schemes are to be compared independently of different channel estimation methods, thus ideal channel estimation is applied. The only constraint is that single carrier equalization should be used because of moderate receiver complexity. The optimal equalization of single time-frequency slots in a WSSUS channel is already given by (6) which is quite too complex for BER performance evaluations. Theoretically the approximation $\mathbf{A}_{g\gamma}(\tau,\nu) \approx$ const. for $(\tau,\nu) \in [0,\tau_d] \times [-B_D, B_D]$ in (8) would be desirable. Then the channel coefficient is given by the Weyl symbol $\mathbf{L}(kF, lT)$ of the channel operator $\boldsymbol{\mathcal{H}}$ sampled at the corresponding

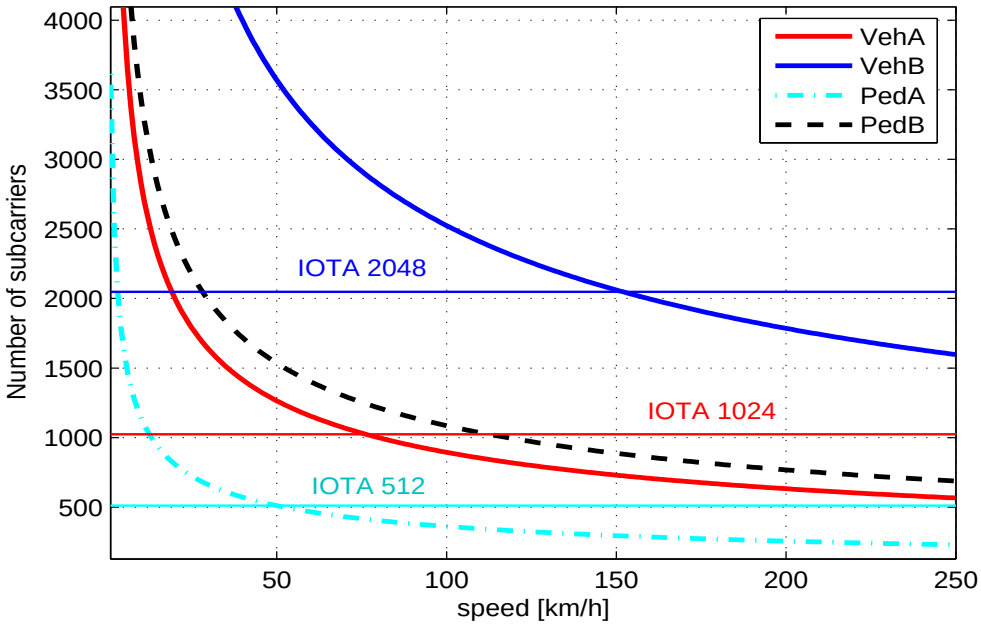

Figure 2: Optimal number of subcarriers that results from the grid scaling rule (i.e. Equ. (12)) under the fixed bandwidth constraint W=7.68 MHz and carrier frequency $f_c = 2GHz$.

time-frequency-slots, i.e.

$$H_{kl,kl} = \int \mathbf{\Sigma}_{\tau\nu} e^{-i2\pi(\tau kF - \nu lT)} d\tau d\nu =: \mathbf{L}(kF, lT) \tag{16}$$

Unfortunately this does not match the way the channel realizations are created in simulation, where the time-variant channel response $h(t,\tau) := \int \Sigma_{\tau\nu} e^{i2\pi\nu t} d\nu$ is given normally. Hence, from practical considerations the following approximation was chosen

$$\begin{aligned} H_{kl,kl} &= \int \overline{g(t)} [\int h(t + lT, \tau) e^{-i2\pi kF\tau} \gamma(t - \tau) d\tau] dt \\ &\approx \int \overline{g(t)} [\int h(lT, \tau) e^{-i2\pi kF\tau} \gamma(t - \tau) d\tau] dt \\ &= \int h(lT, \tau) e^{-i2\pi kF\tau} \mathbf{A}_{g\gamma}(\tau, 0) d\tau \\ &\approx \int h(lT, \tau) e^{-i2\pi kF\tau} d\tau =: \hat{h}(lT, kF) \end{aligned} \tag{17}$$

which is similar to the method proposed in [15]. Note that the latter is a simple cp-OFDM-like ideal channel estimation. We used the following measure δ

$$|\tilde{x}_{kl}^{\text{eq}} - x_{kl}| = |x_{kl}| |\frac{H_{kl,kl}}{\hat{h}(lT,kF)} - 1| =: |x_{kl}|\delta \tag{18}$$

to check the approximation, hence we have to verify that $\delta \ll \frac{1}{2} \min_{ij} |x^{(i)} - x^{(j)}|/|x^{(i)}|$ for a given constellation $\{x^i\}$. For QAM16 that is $\delta \ll 0.3162$.

From Fig.3, Fig.4 and Fig.5 we can conclude that for most of the channel scenarios considered in this paper errors caused by the approximation must have vanishing small probability. Only in Vehicular B channels and Vehicular A/250kmh this additional contribution degrades the performance. We observed that its variance can be up to the order of -32dB. For the other channels the approximation can be used to obtain the ideal BER performance of OQAM/IOTA.

Finally it turns out that if the IOTA-Pulse is correct matched to the channel statistics given by the scattering function the equalization works.

4.2 Notes on Complexity

One of the major advantages of cp-OFDM is its low-complexity FFT-based implementation and equalization (which hold only in time-invariant or slow-fading scenarios). Because equalization of the data carriers (no pilots or virtual carriers) is mandatory we will include it in the characterization of the receiver complexity, i.e. for OFDM with FFT size N we get

$$c_{\text{ofdm}}(N) = 6 \cdot [N/2(\log_2 N - 2) + 1] + 2 \cdot [N \log_2 N] + 17\rho N$$

where ρ accounts for portion of data carriers, i.e. 299/512 for 3GPP proposal OFDM Set 1. We assumed complexities for floating point operations as given table 4.2.

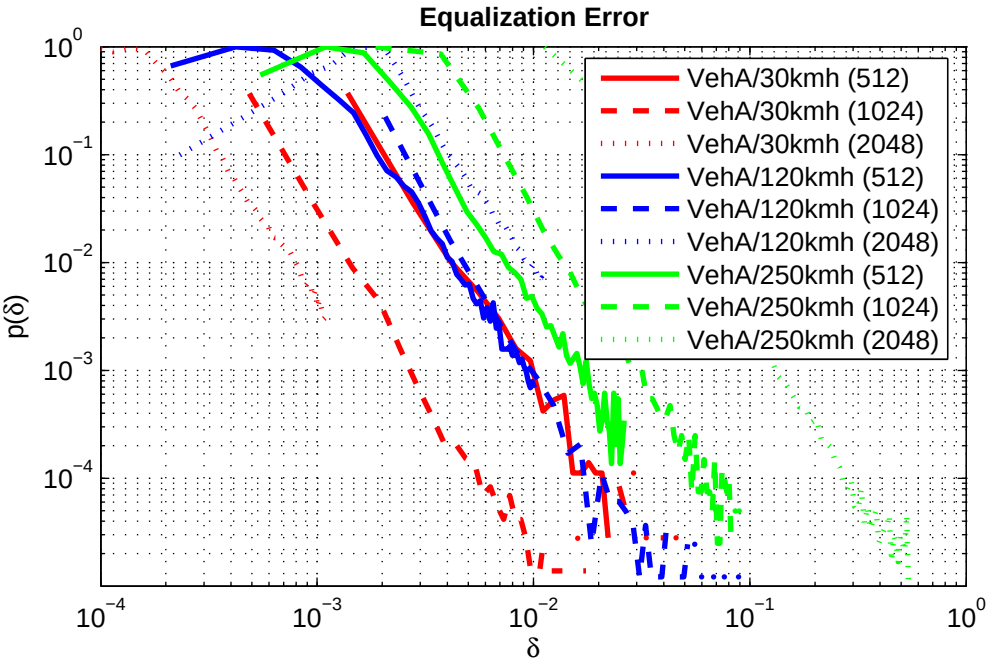

Figure 3: Equalization Error for Vehicular A channel for different mobile speeds and IOTA setups

operation	complexity
real additions and multiplications	1
real divisions	4
complex additions	2
complex multiplications	6
complex divisions	17

Table 1: Basic complexities

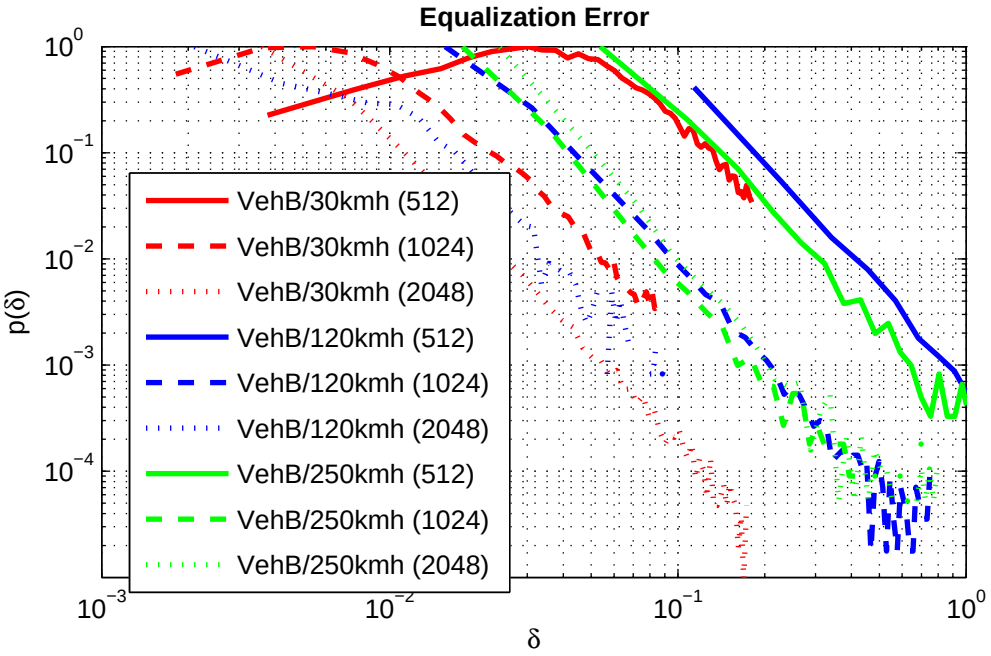

Figure 4: Equalization Error for the Vehicular B channel for different mobile speeds and IOTA setups. Note that only for IOTA 2048 the equalization errors are acceptable small.

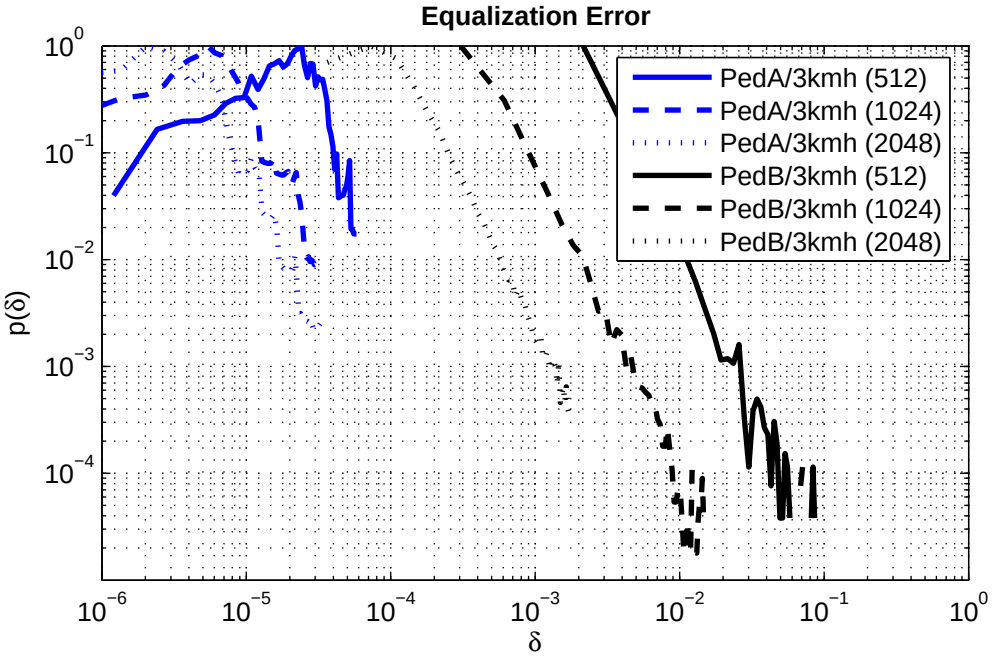

Figure 5: Equalization Error for Pedestrian Channels (A and B) at 3kmh.

For OQAM we like to state that starting from the first implementation proposal by Hirosaki [16] yielding complexity $c_{\mathrm{H}(N,F)}$ for (real) pulse filter length F

$$c_H(N,F) = 10N\log_2 N - 14N + 12 + 8F + 17\rho N$$

further complexity reduction was proposed in [17]. They got nearly half the complexity, i.e.

$$c_V(N,F) = 5N\log_2 N - 5N + 3 + 4F + 17\rho N$$

In (8) and (10) is assumed that the equalization could be done with similar complexity as for cp-OFDM.

In Tab.4.2 the complexity comparison is shown for OQAM/IOTA systems with three different pulses and cp-OFDM. From the figure we can conclude that it is realistic to expect a factor of two in complexity for an OQAM/IOTA implementation with respect to cp-OFDM.

4.3 Coding Issues

OQAM operates exactly at $\varepsilon = 1$ where cp-OFDM at $\varepsilon = \frac{T_u}{T_u+T_{cp}} \approx 0.9$(for the 3GPP OFDM set 1). Hence for comparisons at a fixed information

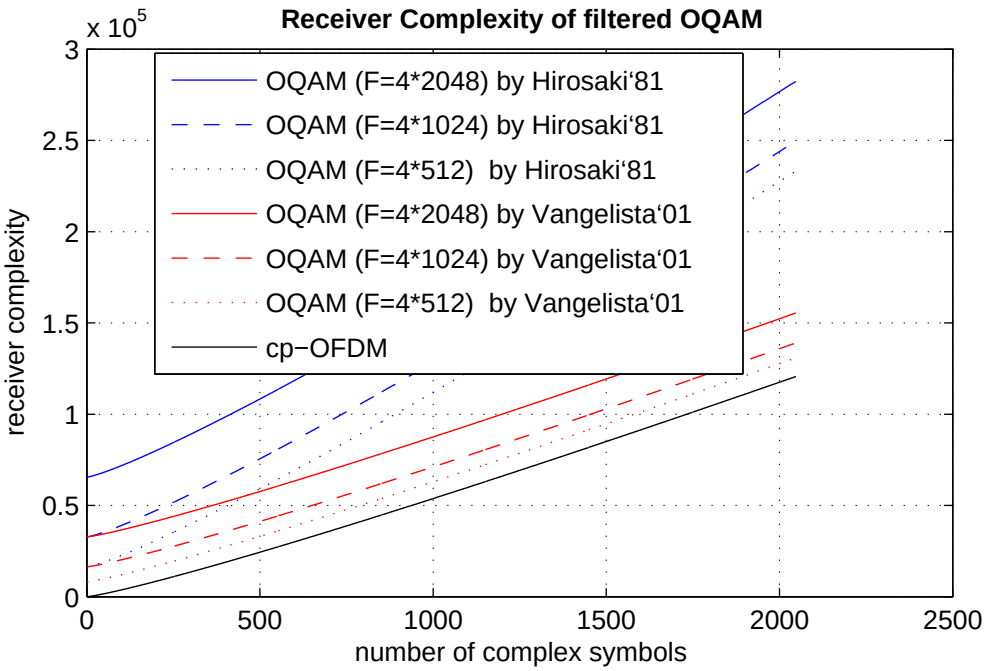

Figure 6: Comparison of the overall receiver complexity of cp-OFDM (c_{ofdm}) and OQAM/IOTA (c_H and c_V) over the number of complex symbols (N) to transmit. The ratio of information bearing carriers to pilots and virtual carriers is assumed to be 299/512.

rate more robust coding can be used for OQAM/IOTA. In particular coding rates of 4/5 for cp-OFDM and 3/4 for OQAM/IOTA (this is a ratio of 93%) exploits most of the additional bandwidth available with OQAM/IOTA.

4.4 UMTS Mask Requirements

Without any filtering OFDM violates the UMTS mask requirement, as shown in Fig.7 for 43dBm case. To fulfil the requirement filtering must be applied (LinearRamp, Postfix), which introduce small (neglectable) intercarrier interference. Due to the rapid spectral decay of IOTA-function the outband emission is much reduced and no further filtering is needed.

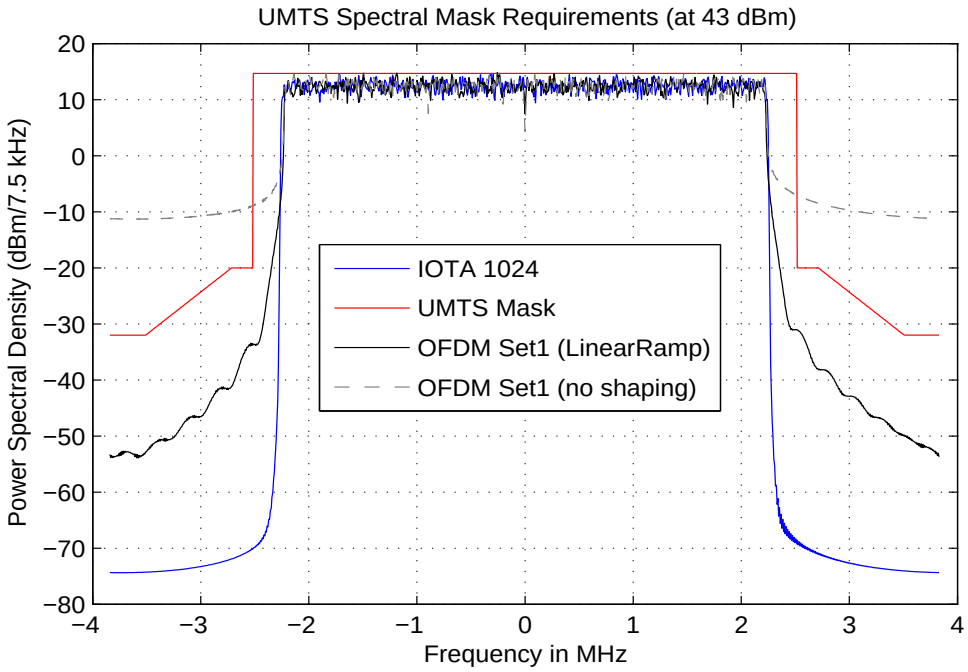

Figure 7: Power spectral density for OFDM Set 1 (299 used subcarriers and FFT size is 512) with and without LinearRamp and IOTA setup using 1024 subcarriers (600 used subcarriers)

Due to the steeper decay of the IOTA spectrum it is possible to increase the used spectrum with respect to OFDM Set 1 where only 299 of total 512 subcarriers can be used for data transmission. For the following comparisons the OFDM scheme was slighty modified to 300 used subcarriers (to get an more common number). In the OQAM modulation only real symbols are transmitted on the subcarriers. It turns out that also for IOTA512 more than 300 subcarriers can be used (for IOTA1024 more than 600, IOTA2048 more than 1200). This is shown in Fig.8. For example in IOTA512 the number

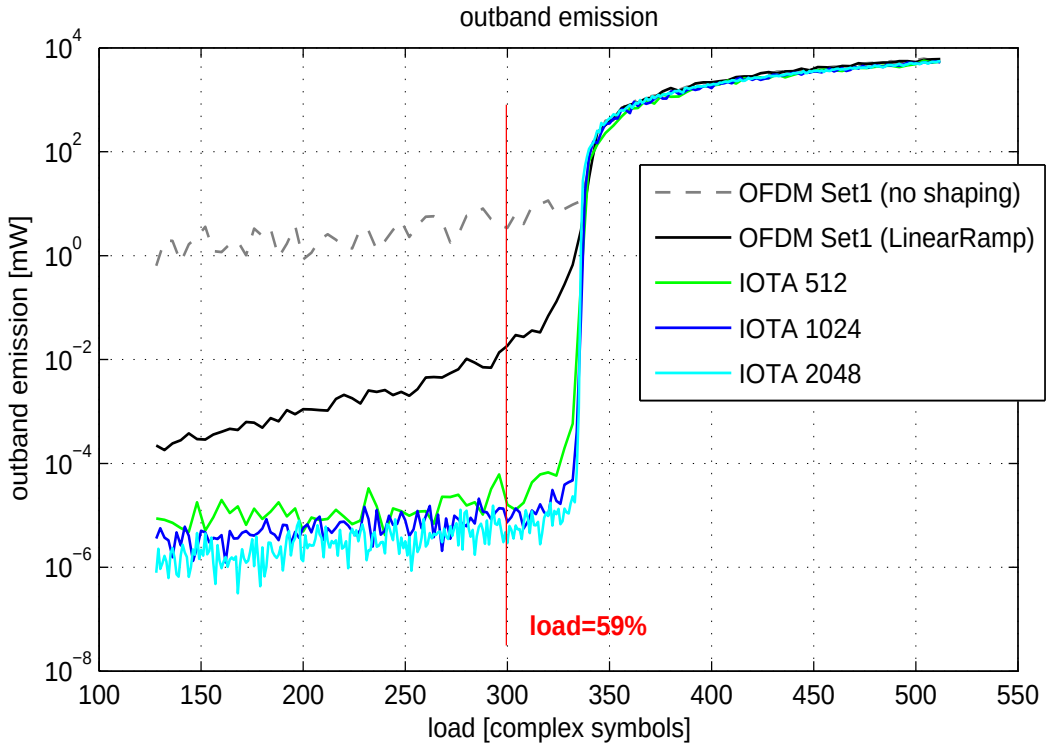

Figure 8: Integrated outband emission in mW for the different multicarrier setups over the number of used complex symbols. For OFDM this is equivalent to the number of subcarriers (the portion of the used spectrum normalized to the number of subcarriers for OFDM is shown here).

could be increased to 316 which increases the overall spectral efficiency of the system. This feature is NOT yet considered here.

4.5 Nonlinear Distortions

Due to the rapid decay of the IOTA function in temporal and spectral domain as well, an decreasing amount outband emission due nonlinear distortions of HPA components can be expected. This was tested with a simple soft delimiter (clipping).

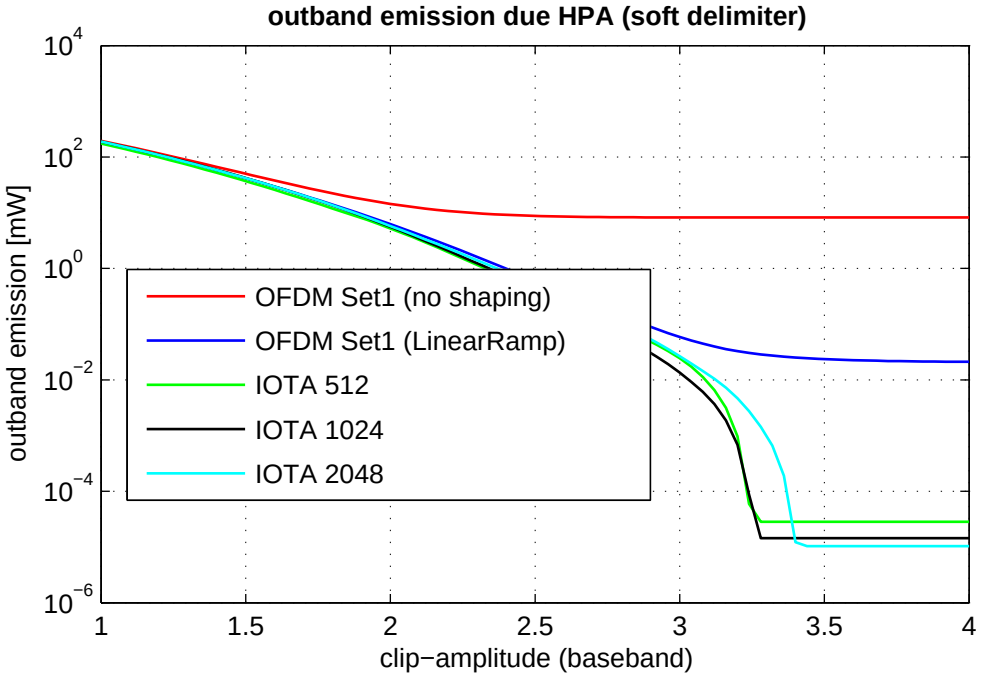

Figure 9: Integrated outband emission for OFDM Set1 (shaped and without shaping) and 3 different IOTA setups due to nonlinear distortion of clipping (soft delimiter, phase stable). The outband emission is integrated for several clipping amplitudes.

It turns out that the saturation of the outband emission depends on the length of IOTA-pulse (L=8 in this case). A more realistic HPA model is the model due Rapp of an SSPA amplifier, given as

$$A(t) = \frac{g \cdot a(t)}{\left[1 + \left(\frac{g \cdot a(t)}{a_{sat}}\right)^{2p}\right]^{\frac{1}{2p}}}$$

where a(t) is the input amplitude and A(t) the output amplitude.

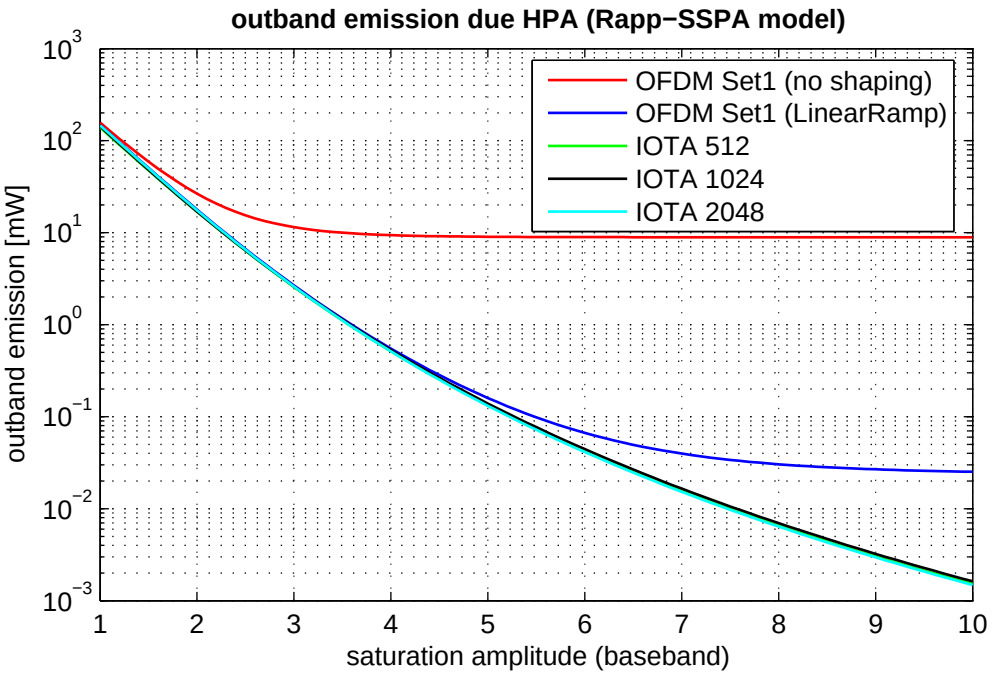

Figure 10: Integrated outband emission for OFDM Set1 (shaped and without shaping) and 3 different IOTA setups due to nonlinear distortion (soft delimiter, phase stable). The outband emission is integrated for several saturation amplitudes (baseband equivalent). Parameters : g=1, p=1.66

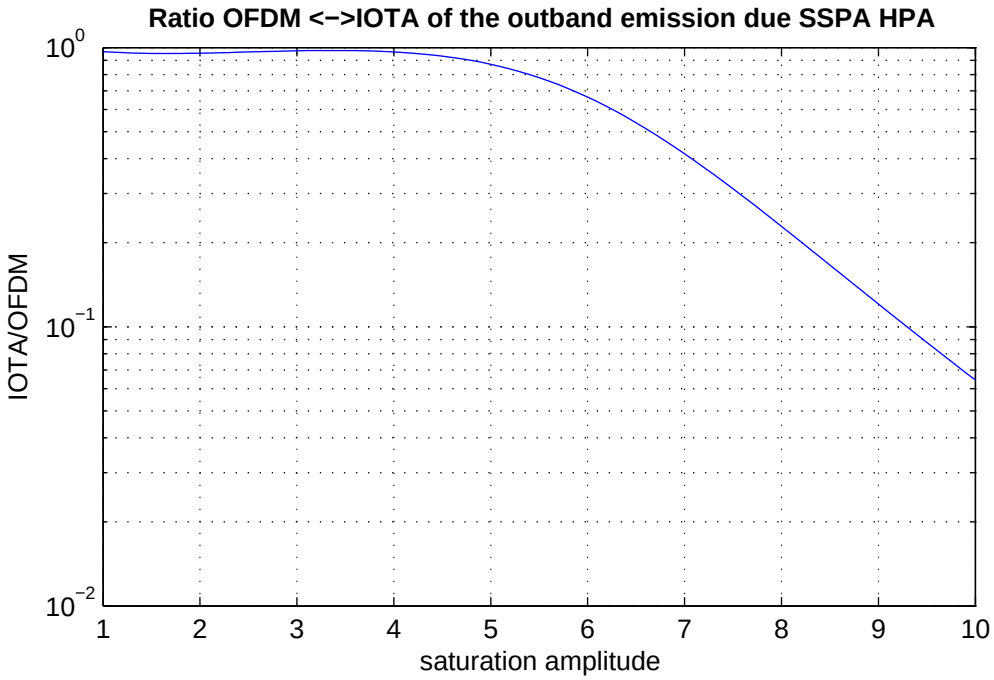

Figure 11: Ratio of integrated outband emission between IOTA1024 and OFDM Set1 (using LinearRamp-Shaping).

5 5. Performance Comparison

5.1 Block Error Rates

We have evaluated the coded performance of the new OQAM/IOTA air interface and conventional cp-OFDM air interface under system constraints that are conform to the 3GPP proposal [2]. We have concentrated on the two major advances provided by the new air interface. OQAM/IOTA should benefit from its higher bandwidth efficiency because more robust coding can be used as in cp-OFDM at the same information rate.

PedA 3kmh	> 4dB achieved at BLER=10ˆ-2
PedB 3kmh	3-4dB achieved at BLER=10ˆ-2
VehA 30kmh	2-3dB achieved at BLER=10ˆ-2 .. 10ˆ-3
VehA 120kmh	ca 2dB achieved at BLER=10ˆ-1
VehA 250kmh	ca 2-3dB achieved at BLER=10ˆ-1..10ˆ-2 (note that OFDM has here an error floor at 10ˆ-3 vor QAM16)

Table 2: Gain of OQAM/IOTA in block error rates (BLER) with respect to cp–OFDM

5.2 Throughput

Moreover, the additional efficiency gain possible due to the reduced out-of-band emission of OQAM/IOTA is now taken into account (300/512 spectral efficiency for OFDM and 312/512 for IOTA). The throughput T can be evaluated as

$$T = (1 - BLER)T_{\max} \tag{19}$$

if the effect of HARQ is neglected. $T_{\max}$is the maximal throughput achieved at BLER=0. In the case of QPSK this is for OFDM = 6.18 Mbit/s and for IOTA = 6.59 Mbit/s. Using QAM16 yields for OFDM = 12.36 Mbit/s and for IOTA = 13.19 Mbit/s. The shift in dB where the maximum throughput of OFDM is achieved with IOTA is given in the following table :

6 Conclusions

An performance evaluation of OQAM/IOTA based air interface in comparison to 3GPP OFDM 1 system design is performed. As main objections the increased efficiency of OQAM/IOTA and the pulse scale adaption in 3GPP context was studied. We conclude that in terms of bit error rates

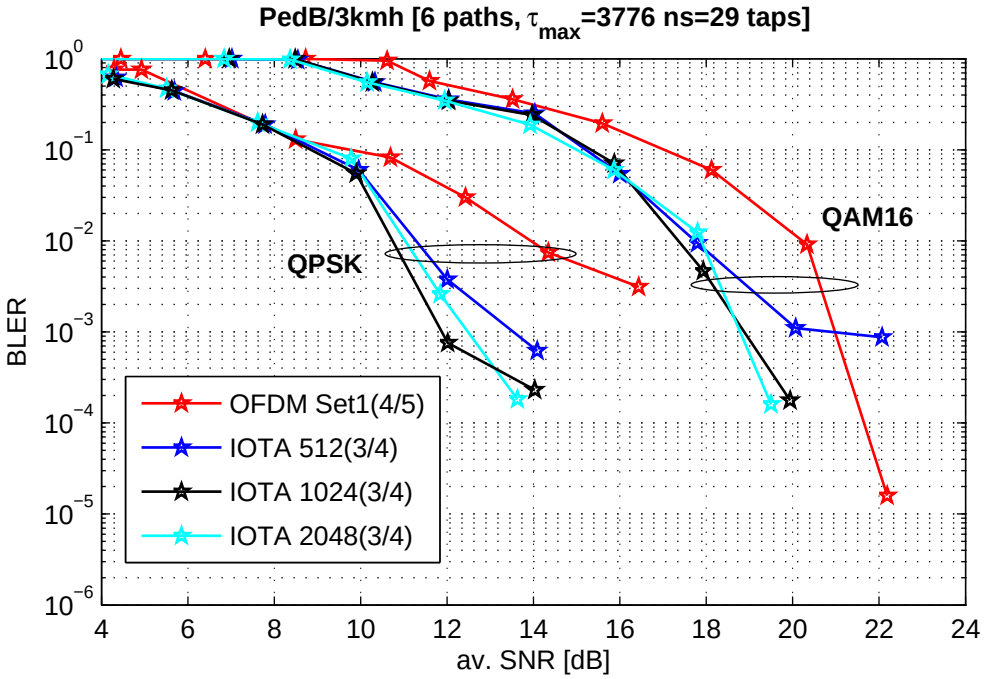

Figure 12: Block Error rates for the Pedestrian B channel at 3km/h for QPSK and QAM. OFDM Set1 has coding rate 4/5 and IOTA uses coding rate 3/4.

	QPSK	QAM16
PedA 3kmh	4..5dB	9dB
PedB 3kmh	4dB	6dB
VehA 30kmh	4dB	6dB
VehA 120kmh	4dB	3..4dB
VehA 250kmh	4dB	6..7dB

Table 3: Gain of OQAM/IOTA in throughput with respect to cp–OFDM

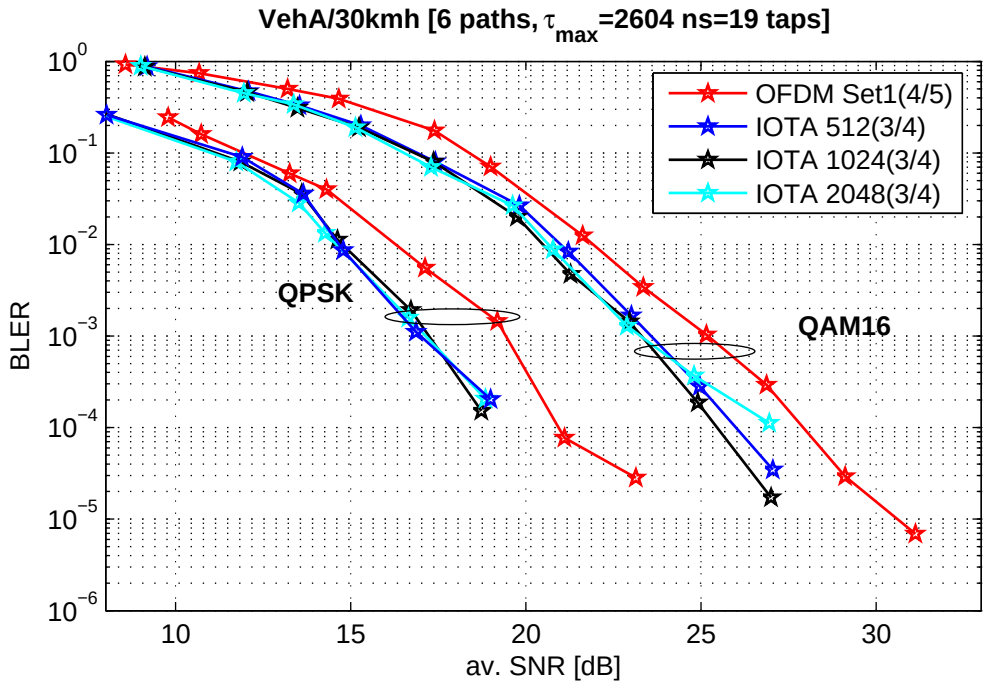

Figure 13: Block Error rates for the Vehicular A channel at 30km/h for QPSK and QAM. OFDM Set1 has coding rate 4/5 and IOTA uses coding rate 3/4.

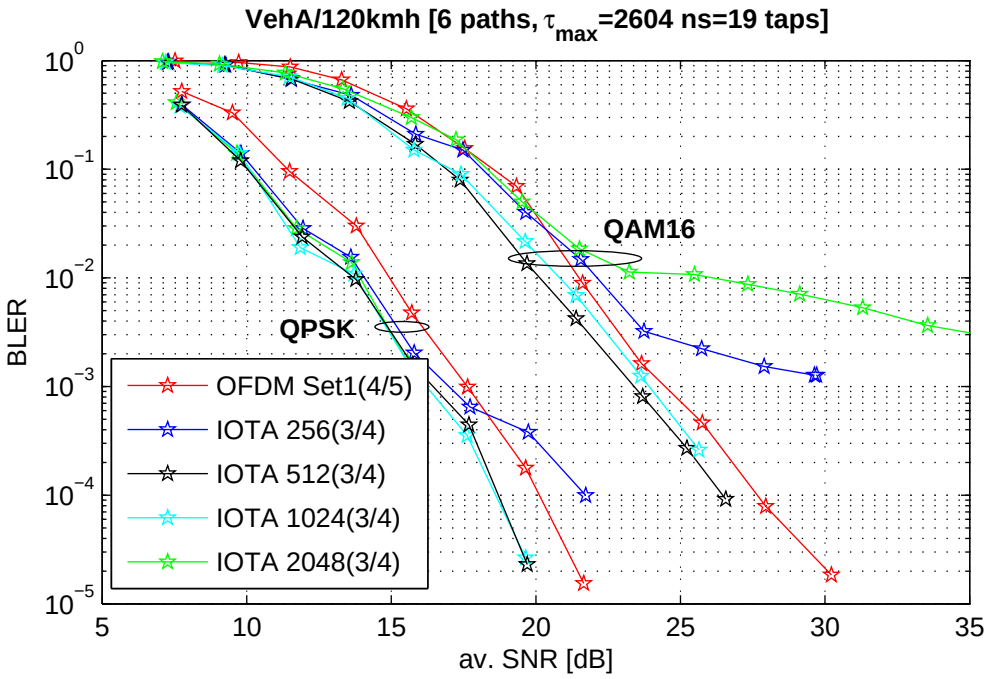

Figure 14: Block Error rates for the Vehicular A channel at 120km/h for QPSK and QAM. OFDM Set1 has coding rate 4/5 and IOTA uses coding rate 3/4.

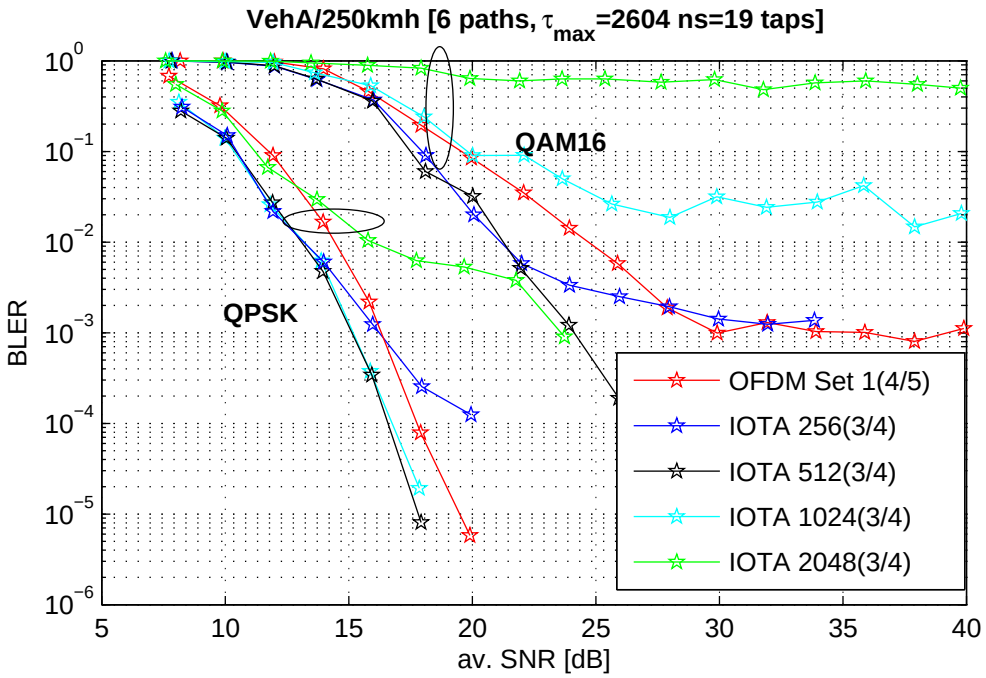

Figure 15: Block Error rates for the Vehicular A channel at 250km/h for QPSK and QAM. OFDM Set1 has coding rate 4/5 and IOTA uses coding rate 3/4.

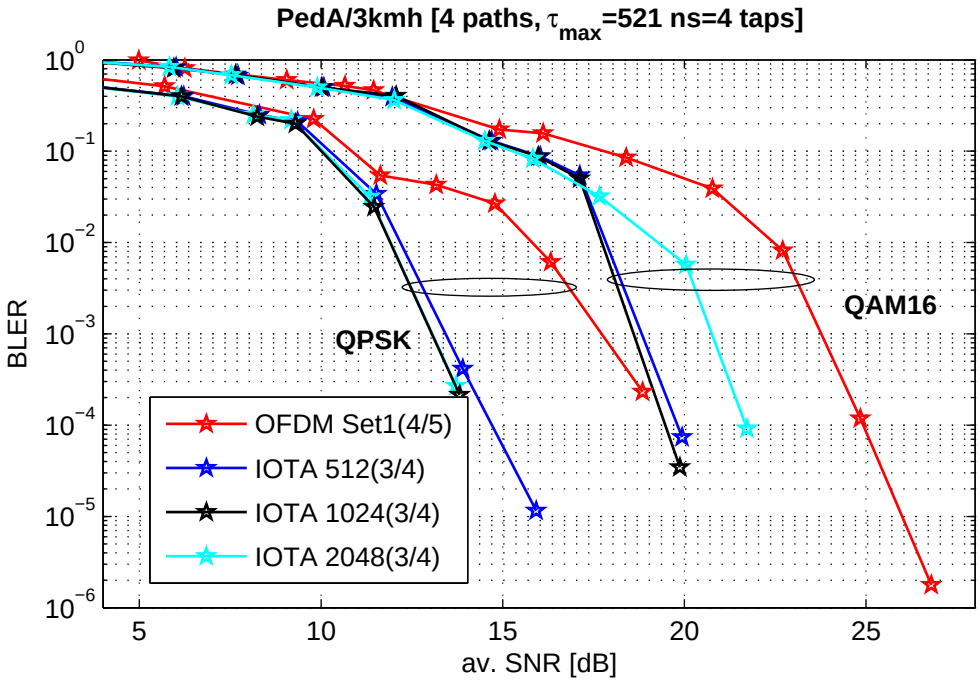

Figure 16: Throughput for the Pedestrian A channel at 3km/h for QPSK and QAM16. OFDM Set1 has coding rate 4/5 and IOTA uses coding rate 3/4.

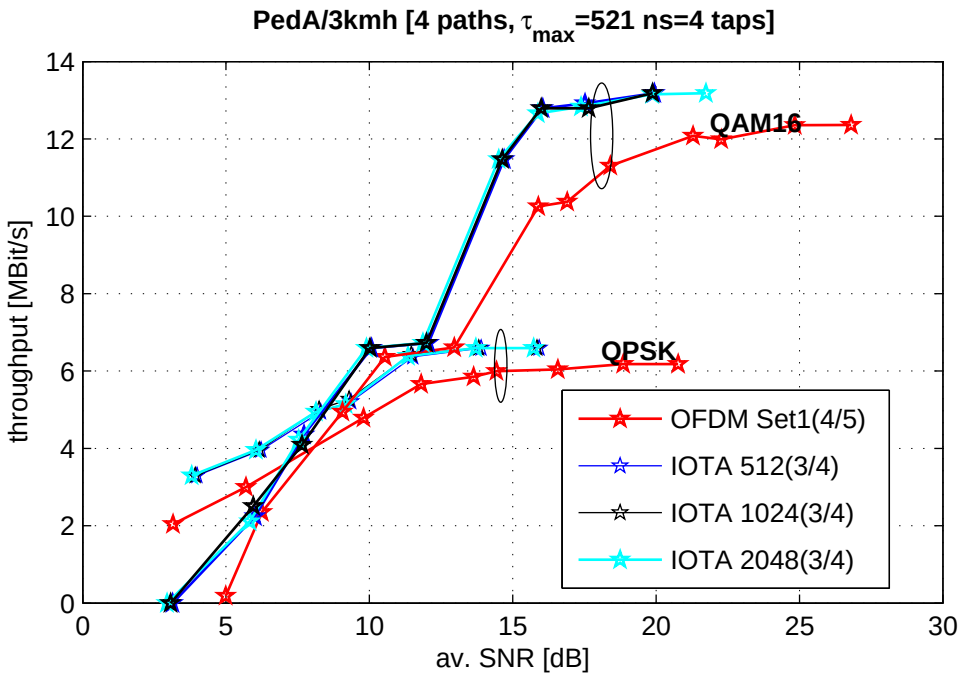

Figure 17: Throughput for the Pedestrian A channel at 3km/h for QPSK and QAM16. OFDM Set1 has coding rate 4/5 and IOTA uses coding rate 3/4.

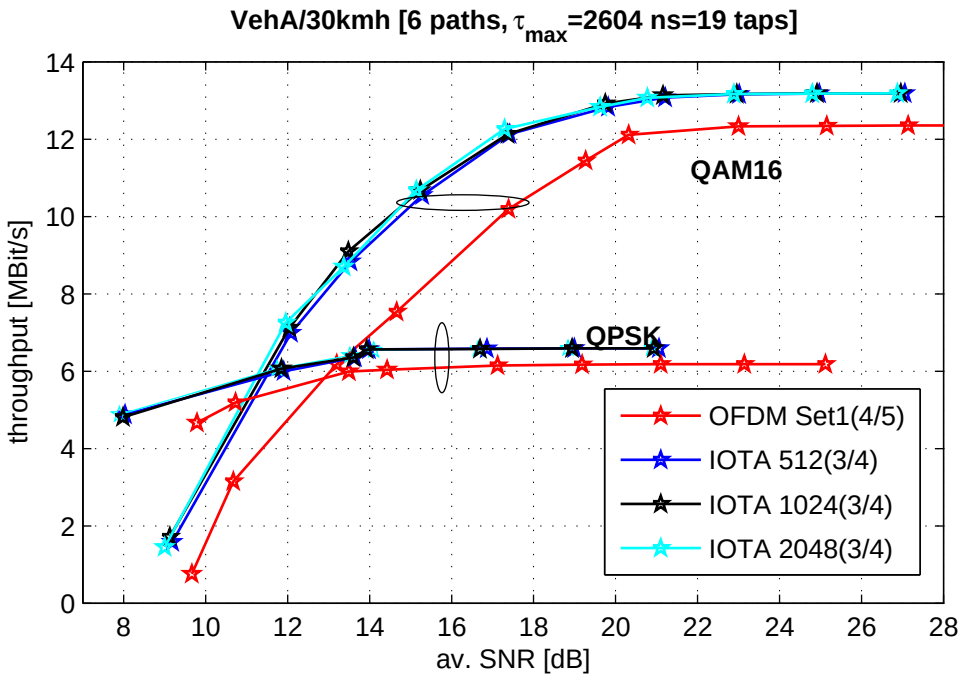

Figure 18: Throughput for the Vehicular A channel at 30km/h for QPSK and QAM16. OFDM Set1 has coding rate 4/5 and IOTA uses coding rate 3/4.

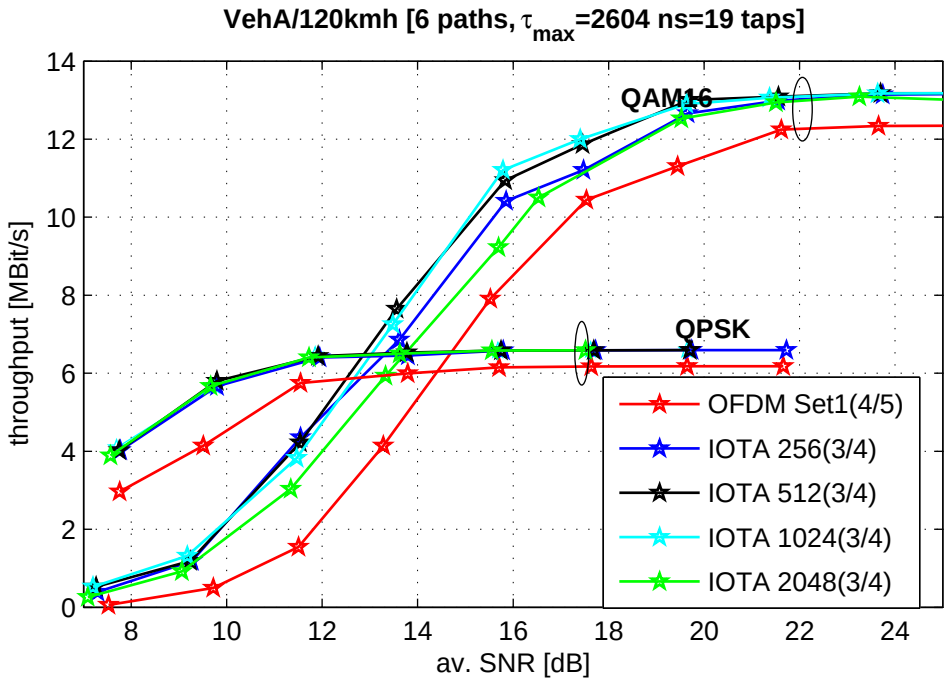

Figure 19: Throughput for the Vehicular A channel at 120km/h for QPSK and QAM16. OFDM Set1 has coding rate 4/5 and IOTA uses coding rate 3/4.

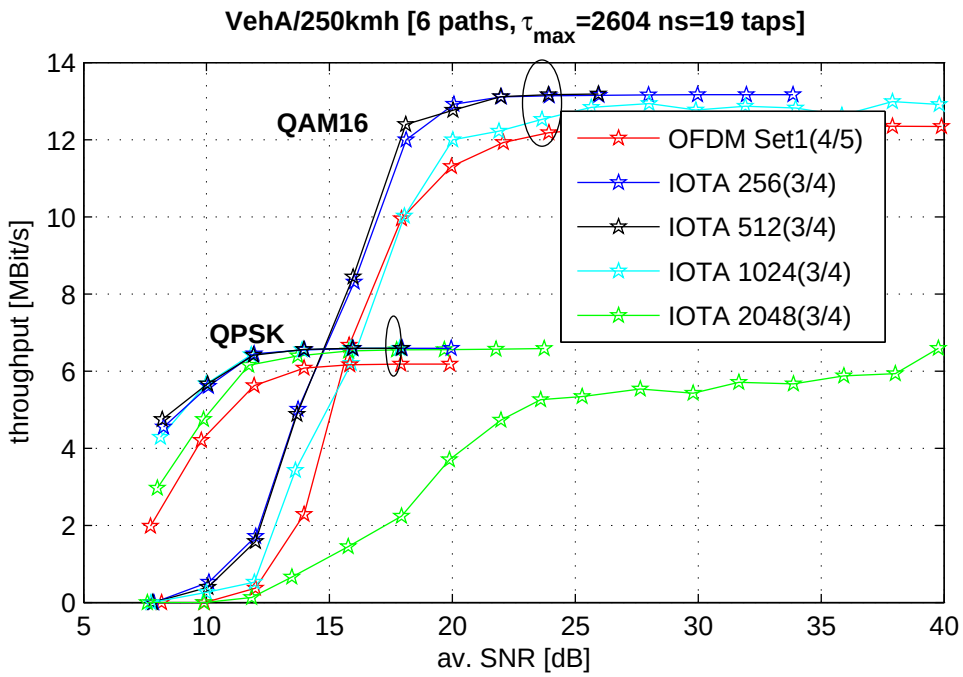

Figure 20: Throughput for the Vehicular A channel at 250km/h for QPSK and QAM16. OFDM Set1 has coding rate 4/5 and IOTA uses coding rate 3/4.

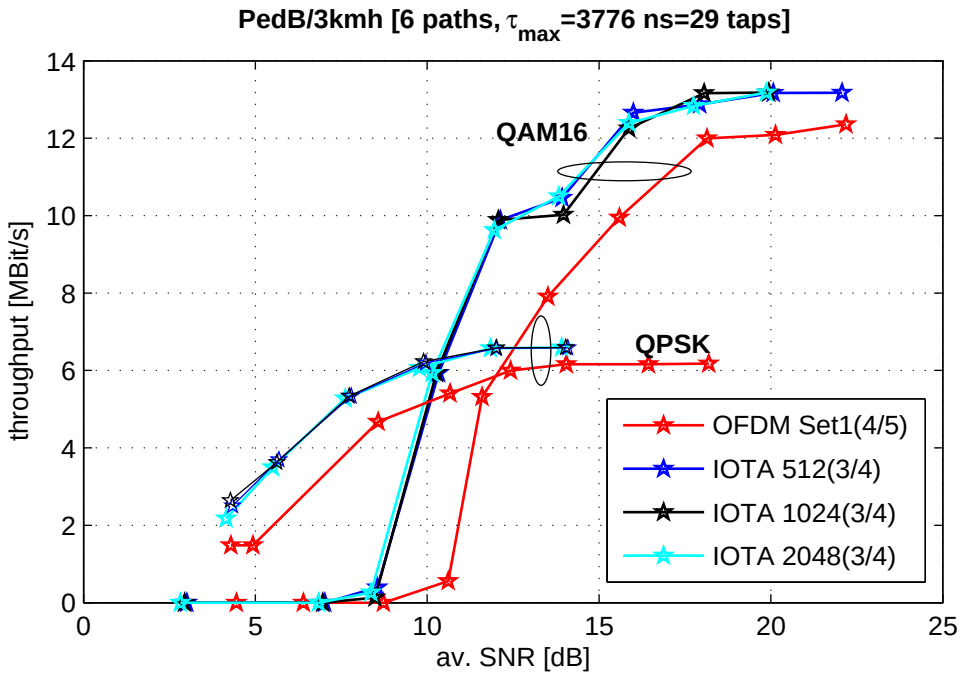

Figure 21: Throughput for the Pedestrian B channel at 3km/h for QPSK and QAM16. OFDM Set1 has coding rate 4/5 and IOTA uses coding rate 3/4.

OQAM/IOTA outperforms cp-OFDM. The latter suffers from its bandwidth loss, its SNR loss and missing adaptivity to given second order statistics of the channel. However, the evolution to OQAM/IOTA comes with slightly higher complexity. Finally we demonstrated that $\tau_d/(2B_D)$ should be included into ongoing discussions on "channel quality information" for OFDM-based HSDPA.

References

[1] B. Classon, P. Sartori, V. Nangia, X. Zhuang, and K. Baum, "Multi-dimensional Adaptation and Multi-user Scheduling Techniques for Wireless OFDM Systems," *International Communications Conference (ICC)*, 2003.

[2] 3GPP TSG-RAN WG1, "TR25.892 Feasibility Study of OFDM for UTRAN Enhancement V1.1.0," *ftp://ftp.3gpp.org/Specs/archive/25_series/25.892*, Mar 2004.

[3] D. Lacroix, N. Goudard, and M. Alard, "OFDM with Guard Interval Versus OFDM/OffsetQAM for High Data Rate UMTS Downlink Transmission," *Vehicular Technology Conference (VTC) 2001 Fall*, vol. 4, pp. 2682–2686, 2001.

[4] I. Daubechies, "Ten Lecures on Wavelets," *Philadelphia, PA: SIAM*, 1992.

[5] R. Chang, "Synthesis of Band-Limited Orthogonal signals for Multicarrier Data Transmission," *Bell. Syst. Tech. J.*, vol. 45, pp. 1775–1796, Dec 1966.

[6] B. Saltzberg, "Performance of an Efficient Parallel Data Transmission System," *IEEE Trans. Commun. Technol.*, vol. COM-15, no. 6, pp. 805–811, Dec 1967.

[7] P. Jung and G. Wunder, "Iterative Pulse Shaping for Gabor Signaling in WSSUS channels," *Fifth IEEE Workshop on Signal Processing Advances in Wireless Communications, Lisboa, Portugal*, 2004. [Online]. Available: ftp://ftp.hhi.de/jungp/publications/Conferences/spawc2004/final.pdf

[8] W. Kozek, "Nonorthogonal Pulseshapes for Multicarrier Communications in Doubly Dispersive Channels," *IEEE Journal on Selected Areas in Communications*, vol. 16, no. 8, pp. 1579–1589, Oct 1998.

[9] ——, "Matched Weyl-Heisenberg expansions of nonstationary environments," *PhD thesis, Vienna University of Technology*, 1996.

[10] S. J. I. Daubechies and J. L. Journe, "A simple Wilson orthonormal basis with exponential decay," *SIAM J. Math. Anal.*, vol. 22, pp. 554–572, 1991.

[11] B. L. Floch, M. Alard, and C. Berrou, "Coded orthogonal frequency division multiplex," *Proceedings of the IEEE*, vol. 83, pp. 982–996, Jun 1995.

[12] A. Janssen and H. Boelcskei, "Equivalence of Two Methods for Constructing Tight Gabor Frames," *IEEE Signal Processing Letters*, vol. 7, no. 4, p. 79, Apr 2000.

[13] T. Strohmer and S. Beaver, "Optimal OFDM Design for Time-Frequency Dispersive Channels," *IEEE Trans. on Communications*, vol. 51, no. 7, pp. 1111–1122, Jul 2003.

[14] H. Bölcskei, P. Duhamel, and R. Hleiss, "Orthogonalization of OFDM/OQAM Pulse Shaping Filters Using the Discrete Zak Transform," *Signal Processing (EURASIP)*, vol. 83, no. 7, pp. 1379–1391, Jul 2003.

[15] D. Lacroix and J. P. Javaudin, "A new channel estimation method for OFDM/OQAM," *7th International OFDM-Workshop, Hamburg*, vol. 2002, 2002.

[16] B. Hirosaki, "An Orthogonally Multiplexed QAM System Using Discrete Fourier Transform," *IEEE Trans. Commun.*, vol. COM-29, pp. 982–989, Jul 1981.

[17] L. Vangelista and N. Laurenti, "Efficient Implementation and Alternative Architectures for OFDM-OQAM Systems," *IEEE Trans. Commun.*, vol. 49, no. 4, pp. 664–675, Apr 2001.